Fuel 234 (2018) 1293–1300

Contents lists available at ScienceDirect

Fuel

journal homepage: www.elsevier.com/locate/fuel

Full Length Article

Effects of pressure and Karlovitz number on the turbulence-flame interactions in lean premixed H_2/air flames

Xujiang Wang[a], Tai Jin[a,b], Yongliang Xie[c], Kai H. Luo[a,*]

[a] Department of Mechanical Engineering, University College London, London WC1E 7JE, UK
[b] State Key Laboratory of Clean Energy Utilization, Zhejiang University, Hangzhou 310027, China
[c] School of Mechanical Engineering, Southwest Jiaotong University, Chengdu 610031, China

ARTICLE INFO

Keywords:
Premixed turbulent flame
Elevated pressure
Turbulence intensity
Flame front structure
Chemical pathway

ABSTRACT

This paper presents three-dimensional direct numerical simulations of lean premixed turbulent H_2/air flames in the thin and distributed reaction zones, with the Karlovitz numbers at 60, 110, 150 and 1000, and pressures at 1 and 5 atm, respectively. Flame front structures and chemical pathways are examined in detail to investigate the effects of pressure and turbulence on flames. There is an increasing number of finer structures on the flame front with increased Karlovitz number. Eddy structures are observed downstream of the reaction zone under high turbulence intensity and thus Karlovitz number, indicating that the turbulent eddies are small and energetic enough to break through the distributed reaction zone. Statistical analysis indicates that the probability of high curvatures increases with increasing Karlovitz number at a constant pressure. When the Karlovitz number is kept constant, the probability of high curvatures is significantly higher at the atmospheric pressure than at elevated pressure. The approximation of Schmidt number (Sc = 1) in theoretical analysis introduces errors in the estimation of the smallest flow scale and the Karlovitz number. Accordingly, in the turbulent flame regime diagram, the boundary between the thin reaction zone and the distributed reaction zone should be modified at the elevated pressure. Moreover, the decorrelation of heat release and H_2 consumption is directly related to turbulence intensity, and the decorrelation is reduced at the elevated pressure. Due to the enhanced radical transport at high Karlovitz number, chemical pathways can be locally changed, which is more significant at elevated pressure.

1. Introduction

Lean premixed turbulent flames are widely used in industrial combustion devices, where the pressure and turbulence intensity tend to be very high. The ratio of turbulence intensity to laminar flame speed is up to 150 in swirl combustors and the pressure can reach more than 30 bar in gas turbines [1,2]. Understanding of flame behaviours at high turbulence intensity and elevated pressure is critical.

Using a non-dimensional Karlovitz number, turbulent premixed flames are classified into flamelet, thin reaction and distributed reaction zones in the combustion regime diagram [3,4]. At high Karlovitz numbers, the smallest turbulence time scale becomes smaller than chemical time scale and scalar mixing is enhanced, which directly modifies the flame structures. Through experimental studies, Driscoll et al. [5,6] discovered that the preheat zone is broadened by increasing turbulence intensity while the thickness of the reaction zone remains relatively constant. No global distributed reaction was observed. Zhou et al. [7,8] investigated methane/air pilot flames from flamelet to distributed reaction zones. Broadened reaction zones, local extinction and homogeneous temperature distribution were reported in the distributed reaction zone. Recently, three-dimensional (3D) direct numerical simulations (DNS) with detailed chemistry are used to study the flame characteristics and chemical pathways at high Karlovitz numbers. Aspden et al. [4,9] conducted a series of lean premixed H_2/air flames and they found that the interface between fuel and products is becoming smooth and there is a decorrelation between heat release and fuel consumption at high Karlovitz numbers. Henning et al. [10] reported fine structures on the flame fronts and clarified the effect of differential diffusion is still significant at high Karlovitz numbers.

It is important to note that the previous studies of high Karlovitz combustion were all conducted at the atmospheric pressure, which have provided valuable information about the interaction of turbulence and flames. On the other hand, most of the industrial combustors are operated under high pressures, where both turbulence and reactions would be significantly modified. Lachaux et al. [11] conducted experiments for lean premixed turbulent methane/air flames at pressure

* Corresponding author.
E-mail address: k.luo@ucl.ac.uk (K.H. Luo).

https://doi.org/10.1016/j.fuel.2018.07.158
Received 17 June 2018; Received in revised form 29 July 2018; Accepted 31 July 2018

up to 0.9 MPa. It was found that the elevated pressure could generate smaller flame structures which would directly increase the flame surface density and reaction rate. The finer structures were also reported by Wang et al. [12,13] for methane and syngas combustion at pressure up to 1.0 MPa. They indicated that the high pressure could increase the frequency of convex structures on the flame front. Increasing efforts of DNS studies of turbulent flames at elevated pressures have also been reported in the literature. Dinesh et al. [14–16] applied 3D DNS to lean premixed expanding spherical flames. More cellular structures were observed, and the turbulent flame speed and heat release increased with the increasing pressure. Savard et al. [17] extended DNS to turbulent combustion of heavy hydrocarbons at 20 bar and they found that the chemical pathways remain globally unchanged at different Karlovitz numbers. However, these experiments and simulations were performed at low or moderate Karlovitz numbers. The characteristics of high Karlovitz flames at elevated pressures are still undocumented.

The aim of present work is to investigate the flame front structures and chemical pathways of turbulent flames at elevated pressures, covering the thin and distributed reaction zones. A series of DNS of lean premixed H_2/air flames with the Karlovitz numbers at 60, 110, 150 and 1000, and pressures at 1 and 5 atm are performed with a detailed chemistry. The paper is organized as follows. Numerical methods and computational parameters are introduced in Section 2. In Section 3, the effects of turbulence intensity and pressure on flame structures and chemical pathways are discussed. Finally, Section 4 presents the conclusions.

2. Numerical approach

2.1. Direct numerical simulation

The 3D simulations performed using the Pencil code [18] solve the time-dependent compressible Navier-Stokes equations coupled with detailed chemical kinetics [19,20]. The governing equations are:

$$\frac{\partial \rho}{\partial t} = -\frac{\partial(\rho u_i)}{\partial x_i} \tag{1}$$

$$\frac{\partial(\rho u_i)}{\partial t} = -\frac{\partial(\rho u_j u_i)}{\partial x_j} - \frac{\partial p}{\partial x_i} + \frac{\partial \tau_{ij}}{\partial x_j} \tag{2}$$

$$\frac{\partial(\rho Y_k)}{\partial t} = -\frac{\partial(\rho u_j Y_k)}{\partial x_j} - \frac{\partial(\rho V_k Y_k)}{\partial x_j} + \dot{\omega} \tag{3}$$

$$\frac{\partial E_T}{\partial t} = -\frac{\partial[(E_T + p)u_j]}{\partial x_j} - \frac{\partial q_j}{\partial x_j} + \frac{\partial(u_j \tau_{ij})}{\partial x_i} \tag{4}$$

where ρ is the mixture density, u_i is the velocity component in x_i direction, p is the pressure and τ_{ij} is the stress tensor. V_k, Y_k and $\dot{\omega}$ are respectively the diffusion velocity, mass fraction and reaction rate for specie k. E_T is the total energy and q_j is the jth-component of heat flux. The mixture is treated as an ideal gas and the equation of state is given by:

$$p = \frac{\rho RT}{MW} \tag{5}$$

where R is the universal gas constant, T is the temperature and MW is the mixture molecular weight. For the species diffusion, Soret and buoyancy effects are neglected, and the mixture-averaged species transport model is adopted, where the species diffusion velocity is expressed as [19]:

$$V_k = -\frac{D_k}{X_k}\left(\nabla X_k + (X_k - Y_k)\frac{1}{p}\nabla p\right) \tag{6}$$

where D_k and X_k are respectively the diffusion coefficient and mole fraction for species k.

The above governing equations are solved with a six-order explicit finite difference scheme in space. Low-storage third-order Runge-Kutta (RK3-2N) scheme is used for time advancement and Livermore Solver for Ordinary Differential Equations (LSODE) is adopted for chemistry calculation. Upwind derivatives are used for convective terms to avoid 'wiggles'. Moreover, helical forcing functions are used to establish required turbulence [21]. The adopted chemical mechanism for H_2/O_2 was developed by Li. et al [22], containing 21 reversible reactions and 9 species. The sample applications of the code in premixed turbulent combustion could be found in [23–25]. The chemistry implementation was validated quantitatively with Chemkin [19,20].

2.2. Simulation parameters

Five 3D DNS cases are performed to study lean premixed H_2/air flames in configurations with an aspect ratio of 2:1:1. Periodic boundary conditions are applied in lateral directions and improved Navier-Stokes Characteristics Boundary Conditions (NSCBC) [26] are applied at the inlet/outlet to maintain the pressure. Due to the high computational cost, the domain width, L, is set to 10 times the integral length scale l_t. This ratio is higher than that reported in Refs. [10,23,24,27,28] with similar configurations. One-dimensional laminar flames and isotropic turbulent boxes were pre-generated to initialize the computational domains. Recalling the relations derived by Peters [3], the five cases locate from the thin reaction zone to the distributed reaction zone as shown in the combustion regime diagram in Fig. 1. Table 1 lists the main simulation parameters. In all cases, the temperature of unburned mixture is $T_u = 298$ K and the equivalence ratio is $\varphi = 0.4$. The laminar flame speed S_L and thickness δ_L were calculated using the same chemical mechanism and transport properties as the turbulent flames. The flame thickness is defined by $\delta_L = (T_b - T_u)/|\nabla T|_{max}$, where T_b is the burnt gas temperature. The turbulent Reynolds number and Karlovitz number are defined as $\mathrm{Re} = (u' l_t)/(S_L \delta_L)$ and $\mathrm{Ka}^2 = (u'/S_L)^3/(l_t/\delta_L)$, where u' is the root-mean-square turbulent velocity fluctuation. Correspondingly, the Kolmogorov length scale is defined as $\eta = l_t\,\mathrm{Re}^{-3/4}$. With the increasing turbulence intensity, η decreases from 49 to 10 μm and the corresponding Ka increases from 60 to 1000. For the three simulations at 5 atm ($P5_L$, $P5_M$ and $P5_H$), the integral length scale is $l_t = 0.0315$ cm, but the turbulence intensity u' varies. For the two simulations at 1 atm, the integral length scale is 0.06 cm. Case $P1_H$ was initialized with the same Ka number as case $P5_H$ and case $P1_M$ was prepared with the same u' as case $P5_H$.

The fine turbulent scales become smaller at high Ka and the flame thickness decreases exponentially with increasing pressure, which requires a higher grid resolution for high Ka flames at elevated pressures [29]. To save computational cost, the l_t/δ_L ratio was kept at unity,

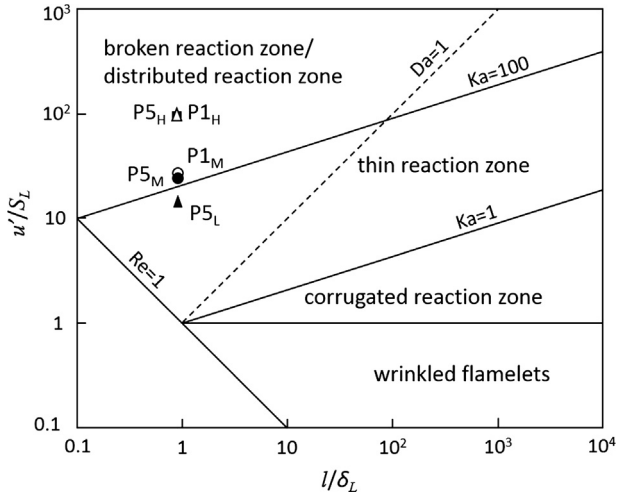

Fig. 1. Simulation cases located in the turbulent combustion regime diagram.

Table 1
Simulation parameters.

Case	P_0 (atm)	S_L (cm/s)	δ_L (cm)	l_t/δ_L	u'/S_L	Δx (μm)	H (μm)	Re	Ka
$P5_L$	5	6.53	0.0315	1	15	8.2	41	15	60
$P5_M$	5	6.53	0.0315	1	23	8.2	30	23	110
$P5_H$	5	6.53	0.0315	1	100	5.5	10	100	1000
$P1_M$	1	23	0.06	1	28	15.6	49	28	150
$P1_H$	1	23	0.06	1	100	10.4	19	100	1000

which was also commonly used in other DNS studies [17,30,31]. There are 38–58 cells across the thickness δ_L and the ratio of cell size to Kolmogorov length scale, $\Delta x/\eta$, is kept below 1.0 to ensure that the smallest turbulence scales are sufficiently resolved. The time step is controlled by the Courant-Friedrichs-Lewy condition for computational stability. Under these resolutions, grid-independent tests were also carried out in two-dimensional DNSs as in our previous work [25]. It indicated that the turbulent flames were well-resolved in space and time. All the simulations are carried out until the mean and statistical values become steady. The simulations were performed with 512–1536 processors on the UK national supercomputing platform ARCHER. The total computational cost for the five cases is around 2.0 million core-hours.

3. Results and discussion

3.1. Flame structures

In turbulent flames, the eddy size determines the interaction between turbulence and the flame front. When the eddy size is characterized with $l_\delta < \eta < \delta_L$, where l_δ is the thickness of inner layer, the small eddies have the ability to penetrate into the reaction zone. At very high Ka when the turbulent flame is supposed to be in the distributed reaction zone, the small-scale vortices are sufficiently energetic to disrupt the reaction zone and even the inner reaction layer. Fig. 2 presents the instantaneous two-dimensional streamlines coloured with temperature contours near the reaction zone. The reaction zone is bounded by non-dimensional progress variable c ($0.1 < c < 0.9$) which is given by:

$$c = (Y_{u,H_2} - Y_{f,H_2})/Y_{u,H_2} - Y_{b,H_2} \quad (7)$$

where Y_{u,H_2} is the H_2 mass fraction in the fresh mixture, Y_{f,H_2} is the local H_2 mass fraction and Y_{b,H_2} is the H_2 mass fraction in the burned gas.

At 5 atm, the flame fronts in all the three cases are highly distorted by large vortices. As the turbulence intensity and consequently Ka increases, smaller vortices become the dominant feature. For case $P5_L$ and $P5_M$, large vortices could be found in the preheat zone ($c < 0.5$). Due to the increased kinematic viscosity at high temperatures, the vortices are substantially suppressed in the reaction zone. As a result, the flow shows laminar characteristics of regular streamlines after the flame front. However, in the high Ka case $P5_H$, a remarkable phenomenon is that many small-scale vortices exist within the preheat zone and reaction zone, which indicates the emergence of the distributed reaction zone. It should be noted that both large and small turbulent eddies could survive after the flame front, unlike the low Ka cases.

The flame structures at 1 atm show similar trends as the cases at 5 atm when Ka is increased. The high Ka flame is characterized by distributed reaction zones with vortices existing within the reaction zone. It is interesting to note that for both cases at 1 atm, vortices survive after the reaction zone. This is due to the fact that the absolute

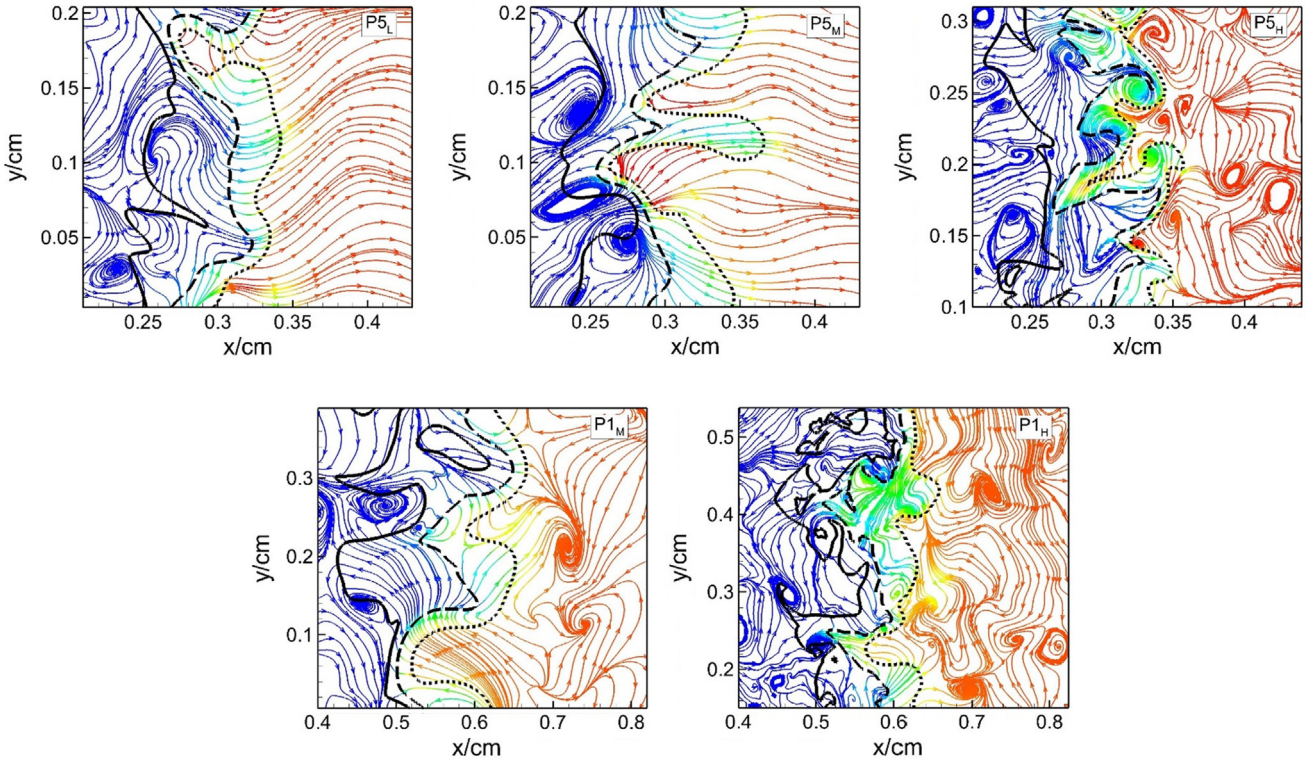

Fig. 2. Instantaneous streamlines coloured with temperature contours near the reaction zone. The solid, dashed and dotted lines correspond to c = 0.1, 0.5 and 0.9, respectively. (For interpretation of the references to colour in this figure legend, the reader is referred to the web version of this article.)

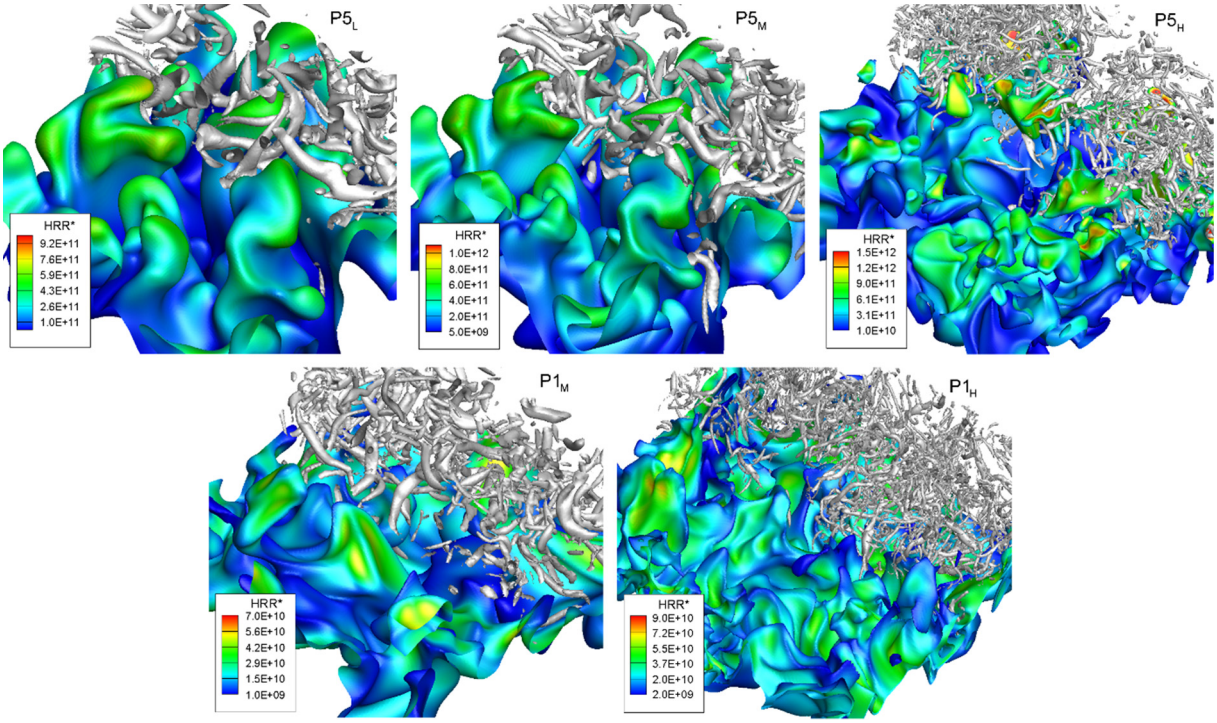

Fig. 3. Iso-surfaces of flame fronts coloured by heat release rate and turbulent vortices defined by $Q^*\_$ criterion ($Q^*\_ = 0.01$) for flames under different turbulence intensities and pressures.

turbulence intensity u' of case $P1_M$ is the same as case $P5_H$. The turbulent eddies are therefore sufficiently energetic to survive across the high-temperature reaction zone. Comparing the two cases $P5_H$ and $P1_H$ with the same Ka, it is found that the upstream and downstream turbulence show similar structures at different pressures, even though the fine turbulence structures are different.

Fig. 3 shows the spatial structures of the premixed flames at different Ka and pressures at the same large eddy turn-over time. The flame front is identified as the temperature iso-surface which corresponds to the maximum temperature gradient, as in [32]. The turbulent vortices are defined by the iso-surfaces of $Q\_$ criterion [33,34]:

$$Q\_ = \frac{1}{2}(\Omega_{ij}\Omega_{ij} - S_{ij}S_{ij}) = -\frac{1}{2}\frac{\partial u_i}{\partial x_j}\frac{\partial u_j}{\partial x_i} > 0 \quad (8)$$

where $S_{ij}$and Ω_{ij} are symmetric and antisymmetric parts of the gradient velocity tensor. As shown in Fig. 3, the vortex structures normalized by u' and η of the unburned mixture are located at the upstream of the flame front at $Q^*\_ = 0.01$ as in [32].

In Fig. 3, all the flame fronts are highly stretched and the convex regions (protruding to unburned mixture) are characterized by high heat release rate (HRR). When turbulence intensity is increased, the peak HRR is enhanced and the $Q\_$ structures become smaller and thinner. Case $P5_L$ and $P5_M$ present quite similar flame fronts and vortex structures. The turbulent eddies are relatively large so that it is difficult for these large structures to enter the flame zone, especially the inner reaction layer. Combined with Fig. 2, these turbulent eddies are significantly dissipated by viscosity in the reaction zone so that few are clearly seen downstream of the flame zone, leading to very regular streamlines.

The two highest Ka cases show different interactions between the turbulent eddies and the reaction zones. The reduced sizes of eddy structures at high turbulence intensity are clearly seen, and similar phenomena were also observed by Day et al. [35] in laboratory-scale flames. The smallest vortical structures are significantly smaller than the apparent structures formed at the distorted flame front. These small eddies are also highly energetic at high turbulence intensity so that they are very likely to enter the flame zone and even the inner reaction layer. Combined with Fig. 2, it becomes clear that a significant portion of turbulent eddies survive the reaction zone, even though the smallest scales may have been dissipated by the high viscosity due to increased temperature. Therefore, the topological structure of the flame front is more “tore apart” at the highest Ka. In the meantime, for the same Ka, the flame structures and turbulent eddy structures at the two different pressures are not easily distinguishable from these plots. However, the ratio of inner layer thickness l_δ to laminar flame thickness δ_L decreases at elevated pressure [36], so turbulent eddy sizes become larger compared with the inner reaction, thus modifying the interaction between the smallest eddies and the inner reaction layer.

3.2. Statistical characteristics

To statistically analyse the flame fronts at different Ka numbers and pressures, Fig. 4 presents the probability density function (PDF) and cumulative distribution function (CDF) of the flame front curvature. The mean curvature is defined as $\kappa = -\nabla\cdot\hat{n}$, where $\hat{n} = -\nabla T/|\nabla T|$ is the unit normal vector of the flame front. The curvature is positive if the surface is protruding to the unburned gas. In Fig. 4, the mean curvature is scaled by the corresponding laminar flame thickness. It shows quantitatively that the probability of high curvatures increases with increasing Ka at any fixed pressure. This is due to the increased small eddies at high turbulence intensity. Moreover, the increase of high positive curvature regions is larger than that of high negative curvature regions. In Fig. 4(b), for the high Ka flame at 1 atm, the cumulative probability of negative curvatures is 0.51, while the value for the same Ka case $P5_H$ is 0.45 at 5 atm. The relative probability of high positive curvature to high negative curvatures is also increased at elevated pressure. It indicates that the convex regions are enlarged when the pressure is elevated, which agrees with the experimental results in [13] and our previous results for flames in the thin reaction zone [25].

As expected, the probability of high curvatures for case $P1_M$ is higher than case $P5_L$ and $P5_M$ due to its higher Ka number. However,

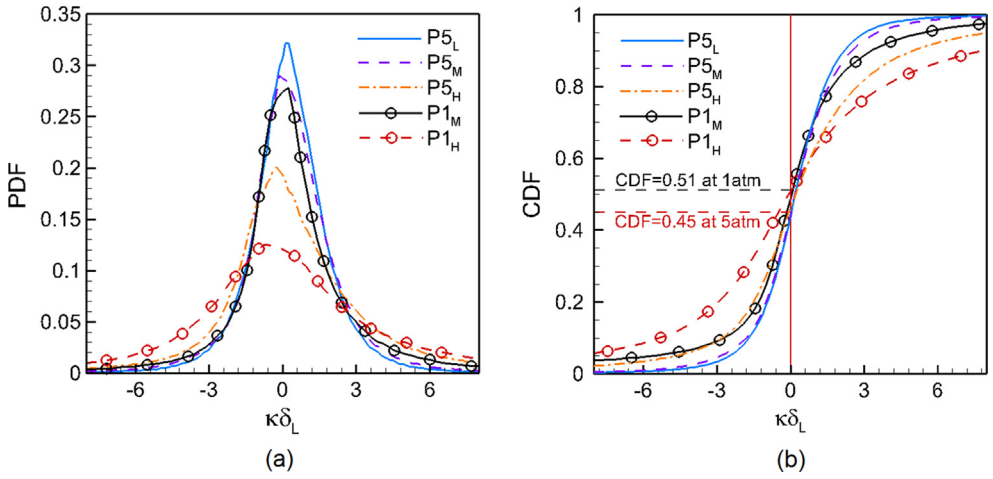

Fig. 4. (a) PDFs and (b) CDFs of mean curvature of flame fronts under different Karlovitz numbers.

the probability of high curvatures for case $P1_H$ is significantly higher than case $P5_H$ despite they have the same Ka number and analogous Q_ structures. It should be noted that the approximate relation $\nu = \mathrm{Sc}\cdot D = D = S_L\cdot\delta_L$ is used in Peters's definition of Re and Ka given that the Schmidt number $\mathrm{Sc} = 1$, where ν is the kinematic viscosity and D is the thermal diffusivity [3]. Nevertheless, the Schmidt number for the H_2/air mixture is around 0.2 instead of 1.

$$\eta = l_t\cdot \mathrm{Re}^{-3/4} = l_t\cdot\left(\frac{u'\cdot l_t}{\nu}\right)^{-3/4} = l_t\cdot\left(\frac{u'\cdot l_t}{Sc\cdot D}\right)^{-3/4} \tag{9}$$

According to Eq. (3), if the real Sc number is adopted in the definition, the ratio η/δ_L for case $P1_H$ is 0.069, while the value for case $P5_H$ is 0.086. It means there are relatively more small-scale vortices for the case at atmospheric pressure. As the high-curvature cusps are induced by small eddies, there should exist larger high-curvature areas in the case $P1_H$. Another reason is that the previously mentioned l_δ/δ_L value decreases significantly with increasing pressure. If this phenomenon is taken in account, the boundary between the thin reaction zone and the broken reaction zone shown in Fig. 1 should move upward at elevated pressures. It indicates that the relative value of Ka at elevated pressure is smaller than that at low pressure when the two cases are located at the same point in the regime diagram.

Fig. 5 presents the distribution of heat release rate against fuel (H2) consumption rate (FCR) on the flame front. At high Ka numbers, the scatters distribute away from the mean values and cover a larger area, which agrees with the findings at atmospheric pressure that the correlation of heat release and H_2 consumption is becoming weaker at high Ka [9,37]. Comparing the cases at different pressures, it is interesting to find that the degree of scatter becomes smaller at the elevated pressure. Moreover, the degree of scatter for case $P1_M$ is analogous to that for case $P5_H$. It is expected that the decorrelation degree of heat release and H_2 consumption is directly related to the turbulence intensity u'. When pressure is elevated, the decorrelation is reduced. Another striking observation is that points with high curvatures (red points) distribute along lower bound and points with low curvatures (blue points) distribute along upper bound of the distribution region. It means that the local convex structures with high positive curvatures are characterized with relatively lower HRR, but the concave structures with high negative curvatures are associated with higher HRR, conditioned on the same FCR. Moreover, the points with the highest curvature values are not located in regions of highest HRR at high turbulence intensity, which corresponds to the effect of the Markstein number [17].

3.3. Chemical pathways

In the present chemical mechanisms for hydrogen, there are 21 reactions. As the interaction between turbulent eddies and reaction zones is changed by the variation of turbulence intensity and pressure, these chemical pathways may also be promoted or suppressed. In order to investigate the effects of pressure and turbulence intensity on the chemical pathways, heat release contributions from main reactions are identified and compared between different cases. Table 2 lists the five main reactions. The total heat release contributions C_{tot} of the main reactions are respectively 86.7% and 87.4% in laminar flames at 1 atm and 5 atm.

Firstly, the global changes in the chemical pathways are identified. Fig. 6 shows the heat release contributions of the main elementary reactions. Two cases at 1 atm ($P1_M$ and $P1_H$) and two cases at 5 atm ($P5_M$ and $P5_H$) are selected for comparison. The heat release contribution is calculated as:

$$C_{hr,i} = \iiint_V q_i dV \Big/ \iiint_V Q dV \tag{10}$$

where q_i is the heat release from reaction i, Q is the total heat release and V is the volume of the computational domain.

At a fixed pressure, there is a big difference between the laminar and turbulent flames, which means the chemical pathways of the laminar flame are modified by turbulence. This phenomenon becomes more significant at the elevated pressure. For the turbulent flames at 5 atm, the heat release contribution of Reaction (8) (R8) increases 8% while the contribution of Reaction (13) (R13) decreases 10%. When the pressure is elevated, R8 and R13 are promoted while Reaction (9) (R9) and Reaction (11) (R11) are suppressed for the turbulent flames. Nevertheless, Reaction (3) (R3) is less sensitive to both pressure and turbulence intensity in the studied cases. With increasing turbulence intensity, the contribution of R8 decreases and the contribution of R9 increases slightly at both pressures. However, the effect of turbulence intensity shows opposite trend for R11 and R13 at the two pressures. It is found in Ref. [17] that the global heat release contribution from each reaction step is independent of Ka at a fixed pressure. In comparison, larger deviations can be found between different Ka cases in the present study, especially at 5 atm. However, the maximum difference is 2.8%, which indicates that the effects of turbulence intensity on global heat release contributions from each reaction step are still limited for flames in the distributed reaction zone.

Secondly, it is of great interest to examine the distribution of local heat release contributions given that the global contribution is sensitive to pressure while insensitive to turbulence intensity. Fig. 7 gives the relative heat release (HR_r) contributions of the most contributing reactions versus progress variable c. In this plot, the heat release contribution is conditioned by Eq. (4) to eliminate the effects of enhanced volumetric heat release at high pressure and turbulence intensity.

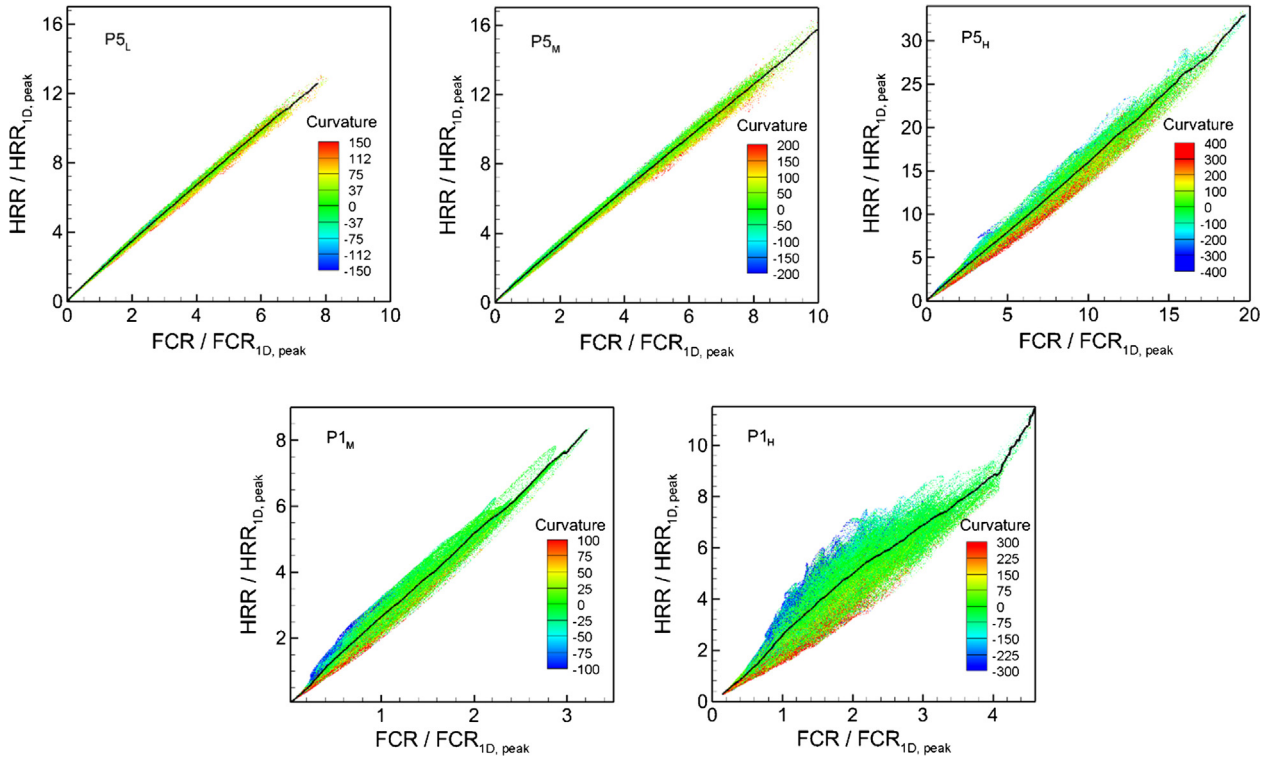

Fig. 5. Scatter plots of normalized heat release rate and H_2 consumption rate on the flame fronts coloured by mean curvature. The solid line denotes the mean values.

Table 2
Main reactions of Li et al. H_2/O_2 mechanism.

#	Reaction	#	Reaction
R3	$H_2 + OH = H_2O + H$	R8	$H + OH + M = H_2O + M$
R9	$H + O_2 (+M) = HO_2 (+M)$	R11	$HO_2 + H = OH + OH$
R13	$HO_2 + OH = H_2O + O_2$		

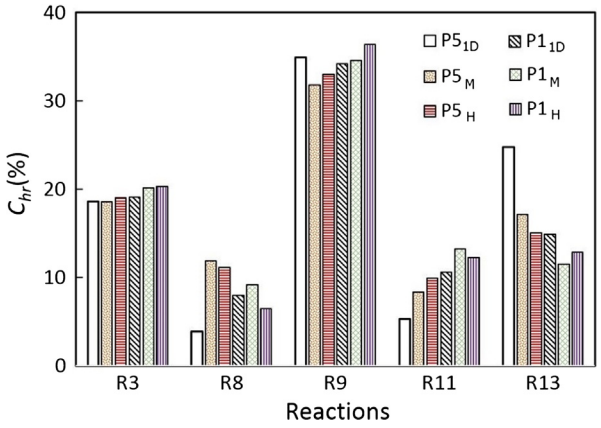

Fig. 6. Heat release contributions of main reactions for the laminar and turbulent flames.

Although the heat release rate is higher at high Ka number, it does not mean the HR_r value is also higher. HR_r means the heat release contribution rate (HRCR) of different pathways other than the heat release rate.

$$C_{hr,i} = \int_0^1 HR_{r,i}\,dc \tag{11}$$

where i means the reaction number.

In Fig. 7, it is evident that chemical pathways are locally changed by turbulence and pressure. At atmospheric pressure, the HRCRs of R9 and R13 are enhanced when $c < 0.7$, while the enhancements of R3, R8 and R11 are not significant for the high Ka case $P1_H$. In the intense reaction regions ($c > 0.7$), the contribution rates of R8, R9 and R11 are dramatically decreased. It is also noted that the contribution rate of R3 is locally independent of turbulence intensity at atmospheric pressure. When the pressure is elevated to 5 atm, the effects of turbulence become more evident. At $c < 0.9$, all the selected reactions are significantly promoted at high Ka, while these reactions are suppressed in the high-intensive reaction regions. Note that theses reaction contribution rates are modified by different degrees at the same c value, which illustrates the different effects of turbulence on different chemical pathways.

In these cases, the weak reaction regions correspond to low temperatures and the intense reaction regions correspond to high temperatures. Comparing the cases at different pressures, the overall effect of turbulence intensity is the same. The reactions will be promoted at low-temperature regions and suppressed at high-temperature regions when the turbulence intensity is increased. The reaction zone is therefore thickened. It can be attributed to enhanced radical distribution through turbulent convection. The concentrations of H, O, OH, HO_2, etc will be increased in low-temperature regions and as a result the heat release contribution rates are increased. However, significant differences are observed under different pressures. The demarcation points change from around $c = 0.7$ under 1 atm to $c = 0.9$ under 5 atm. Moreover, the contribution rates at low and moderate progress variable values are relatively lower at the elevated pressure. As aforementioned, the inner layer in the reaction zone is dramatically decreased at high pressure. It is also known that most of the radical production happens in the inner layer. Therefore, it becomes harder for small eddies to penetrate into the inner layer and transport species to the low-temperature regions when the pressure is elevated.

4. Conclusions

DNS of lean premixed turbulent H_2/air flames in the thin and distributed reaction zones are performed at different pressures. The effects

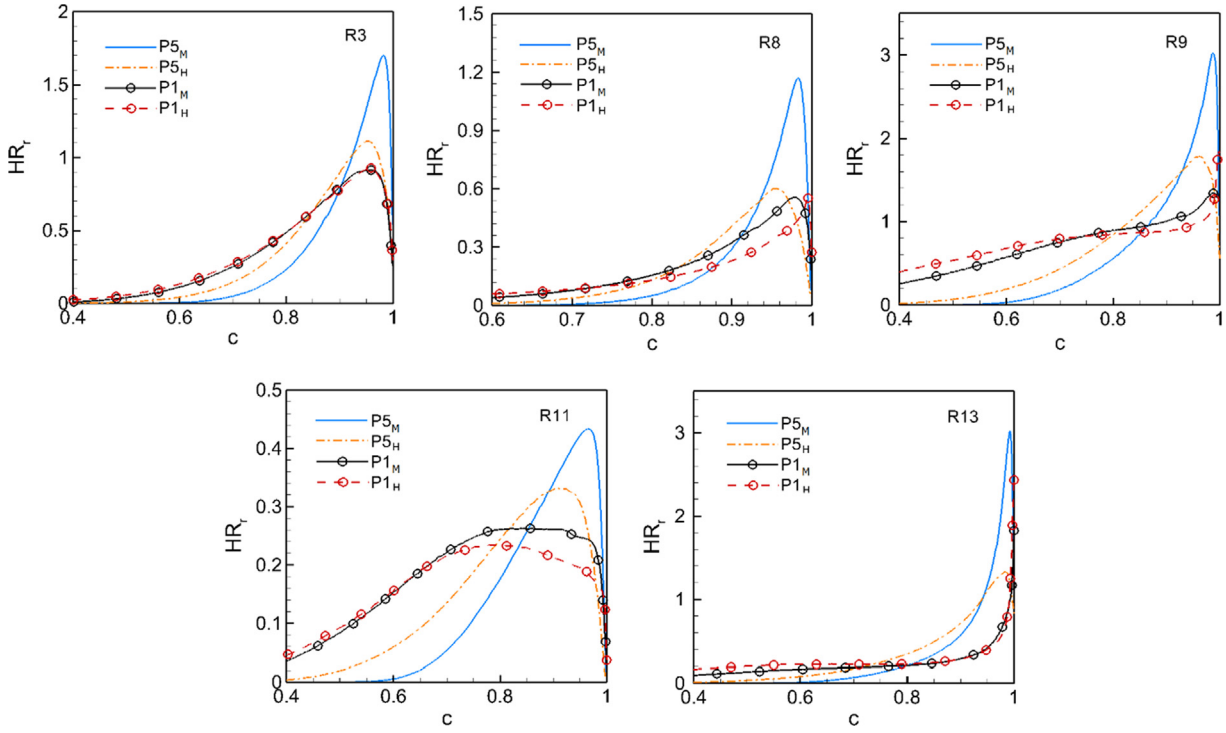

Fig. 7. Relative heat release contributions of individual elementary reaction versus progress variable for flames at moderate and high Ka numbers.

of pressure and turbulence intensity on flame structures are assessed qualitatively and quantitatively. Moreover, the influences of pressure and turbulence on chemical pathways are identified globally and locally.

At high Ka, there are many small vortices in the preheat zone, which are sufficiently energetic to disrupt the reaction zone. As a result, the flame fronts are seriously distorted and exhibit complex topological structures with small pockets. A significant portion of turbulent eddies are substantially suppressed in the reaction zone due to high viscosity. Nevertheless, eddy structures can be observed downstream the reaction zone under high turbulence intensity and thus high Ka, indicating that the turbulent eddies are small and energetic enough to break through the distributed reaction zone.

Statistical analysis identifies that the probability of high curvatures increases with increasing Ka at a certain pressure. When Ka is kept constant, the probability of high curvatures is significantly higher at the atmospheric pressure. The approximation of Schmidt number (Sc = 1) in theoretical analysis introduces errors in the estimation in the smallest flow thickness and the Karlovitz number. These findings suggest the necessity for modification of Peters's regime diagram at elevated pressures, which is an interesting area for future investigation. The decorrelation of heat release and H_2 consumption is directly related to the turbulence intensity u' and the decorrelation is reduced at elevated pressure. It is interesting to find that under the same H_2 consumption rate, heat release rates in regions with high positive curvatures are relatively lower, compared with regions with high negative curvatures.

Although the effects of pressure and turbulence intensity on global heat release contribution are limited, the chemical pathways can be changed locally. Overall, the major reactions are promoted at moderate-temperature regions and suppressed at high-temperature regions when turbulence intensity is increased. However, the changing rates are different for different elementary reactions at the same progress variable. It is also found that the effects of pressure on the modification of local chemical pathways are significant. Since the inner layer is thinner at elevated pressure, radical convection by small eddies is reduced. As a result, reaction contribution rates in moderate-temperature regions are apparently lower than those at the atmospheric pressure. Therefore, further increasing pressure to levels relevant to industrial combustion devices will be an important and interesting area for future investigation.

Acknowledgements

This work was supported by the UK Engineering and Physical Sciences Research Council under the projects "UK Consortium on Mesoscale Engineering Sciences (UKCOMES)" (Grant Nos. EP/L00030X/1 and EP/R029598/1) and "High Performance Computing Support for United Kingdom Consortium on Turbulent Reacting Flow (UKCTRF)" (Grant No. EP/K024876/1). Sponsorships for Mr Xujiang Wang by University College London and China Scholarship Council are gratefully acknowledged. Tai Jin acknowledges the financial support by the National Natural Science Foundation of China (No. 51576176).

References

[1] Strakey P, Sidwell T, Ontko J. Investigation of the effects of hydrogen addition on lean extinction in a swirl stabilized combustor. Proc Combust Inst 2007;31(2):3173–80.
[2] Goswami M, van Griensven JGH, Bastiaans RJM, Konnov AA, de Goey LPH. Experimental and modeling study of the effect of elevated pressure on lean high-hydrogen syngas flames. Proc Combust Inst 2015;35(1):655–62.
[3] Peters N. Turbulent combustion. Cambridge: Cambridge University Press; 2000.
[4] Aspden AJ, Day MS, Bell JB. Turbulence–flame interactions in lean premixed hydrogen: transition to the distributed burning regime. J Fluid Mech 2011;680:287–320.
[5] Driscoll JF. Premixed turbulent combustion in high reynolds number regimes of thickened flamelets and distributed reactions. AFOSR and ARO basic combustion research review. University of Michigan; 2016.
[6] Temme JE, Skiba A, Wabel T, Driscoll JF. Premixed turbulent combustion in high reynolds number regimes – of thickened flamelets and distributed reactions. 8th U.S. national combustion meeting. University of Utah; 2013.
[7] Zhou B, Brackmann C, Li Q, Wang Z, Petersson P, Li Z, et al. Distributed reactions in highly turbulent premixed methane/air flames. Combust Flame 2015;162(7):2937–53.
[8] Zhou B, Brackmann C, Li Z, Aldén M, Bai X-S. Simultaneous multi-species and temperature visualization of premixed flames in the distributed reaction zone regime. Proc Combust Inst 2015;35(2):1409–16.
[9] Aspden AJ, Day MS, Bell JB. Turbulence-chemistry interaction in lean premixed hydrogen combustion. Proc Combust Inst 2015;35(2):1321–9.
[10] Carlsson H, Yu R, Bai X-S. Direct numerical simulation of lean premixed CH_4/air

and H_2/air flames at high Karlovitz numbers. Int J Hydrogen Energy 2014;39(35):20216–32.
[11] Lachaux T, Halter F, Chauveau C, Gökalp I, Shepherd IG. Flame front analysis of high-pressure turbulent lean premixed methane–air flames. Proc Combust Inst 2005;30(1):819–26.
[12] Wang J, Yu S, Zhang M, Jin W, Huang Z, Chen S, et al. Burning velocity and statistical flame front structure of turbulent premixed flames at high pressure up to 1.0 MPa. Exp Therm Fluid Sci 2015;68:196–204.
[13] Wang J, Zhang M, Huang Z, Kudo T, Kobayashi H. Measurement of the instantaneous flame front structure of syngas turbulent premixed flames at high pressure. Combust Flame 2013;160(11):2434–41.
[14] Ranga Dinesh KKJ, Shalaby H, Luo KH, van Oijen JA, Thévenin D. High hydrogen content syngas fuel burning in lean premixed spherical flames at elevated pressures: effects of preferential diffusion. Int J Hydrogen Energy 2016;41(40):18231–49.
[15] Ranga Dinesh KKJ, Shalaby H, Luo KH, van Oijen JA, Thévenin D. Effects of pressure on cellular flame structure of high hydrogen content lean premixed syngas spherical flames: a DNS study. Int J Hydrogen Energy 2016;41(46):21516–31.
[16] Ranga Dinesh KKJ, Shalaby H, Luo KH, van Oijen JA, Thévenin D. Heat release rate variations in high hydrogen content premixed syngas flames at elevated pressures: effect of equivalence ratio. Int J Hydrogen Energy 2017;42(10):7029–44.
[17] Savard B, Lapointe S, Teodorczyk A. Numerical investigation of the effect of pressure on heat release rate in iso-octane premixed turbulent flames under conditions relevant to SI engines. Proc Combust Inst 2017;36(3):3543–9.
[18] http://pencil-code.nordita.org/. The Pencil Code.
[19] Babkovskaia N, Haugen NEL, Brandenburg A. A high-order public domain code for direct numerical simulations of turbulent combustion. J Comput Phys 2011;230(1):1–12.
[20] Kee RJ, Rupley FM, Meeks E, Miller JA. CHEMKIN-III: a FORTRAN chemical kinetics package for the analysis of gas-phase chemical and plasma kinetics. Sandia national laboratories report SAND96-8216. 1996.
[21] Brandenburg A. The inverse cascade and nonlinear alpha-effect in simulations of isotropic helical hydromagnetic turbulence. Astrophys J 2001;550(2):824–40.
[22] Li J, Zhao Z, Kazakov A, Dryer FL. An updated comprehensive kinetic model of hydrogen combustion. Int J Chem Kinet 2004;36(10):566–75.
[23] Chaudhuri S. Life of flame particles embedded in premixed flames interacting with near isotropic turbulence. Proc Combust Inst 2015;35(2):1305–12.
[24] Uranakara HA, Chaudhuri S, Dave HL, Arias PG, Im HG. A flame particle tracking analysis of turbulence–chemistry interaction in hydrogen–air premixed flames. Combust Flame 2016;163:220–40.
[25] Wang X, Jin T, Xie Y, Luo KH. Pressure effects on flame structures and chemical pathways for lean premixed turbulent H_2/air flames: three-dimensional DNS studies. Fuel 2018;215:320–9.
[26] Lodato G, Domingo P, Vervisch L. Three-dimensional boundary conditions for direct and large-eddy simulation of compressible viscous flows. J Comput Phys 2008;227(10):5105–43.
[27] Carlsson H, Yu R, Bai X-S. Flame structure analysis for categorization of lean premixed CH_4/air and H_2/air flames at high Karlovitz numbers: direct numerical simulation studies. Proc Combust Inst 2015;35(2):1425–32.
[28] Wang Z, Motheau E, Abraham J. Effects of equivalence ratio variations on turbulent flame speed in lean methane/air mixtures under lean-burn natural gas engine operating conditions. Proc Combust Inst 2017;36(3):3423–30.
[29] Yao T, Yang WH, Luo KH. Direct numerical simulation study of hydrogen/air autoignition in turbulent mixing layer at elevated pressures. Comput Fluids 2018.
[30] Savard B, Bobbitt B, Blanquart G. Structure of a high Karlovitz n-C_7H_{16} premixed turbulent flame. Proc Combust Inst 2015;35(2):1377–84.
[31] Lapointe S, Savard B, Blanquart G. Differential diffusion effects, distributed burning, and local extinctions in high Karlovitz premixed flames. Combust Flame 2015;162(9):3341–55.
[32] Yenerdag B, Fukushima N, Shimura M, Tanahashi M, Miyauchi T. Turbulence–flame interaction and fractal characteristics of H_2–air premixed flame under pressure rising condition. Proc Combust Inst 2015;35(2):1277–85.
[33] Lai H, Luo KH. A three-dimensional hybrid LES-acoustic analogy method for predicting open-cavity noise. Flow Turbu Combust 2007;79(1):55–82.
[34] Hunt JC, Wray AA, Moin P. Eddies, streams, and convergence zones in turbulent flows. Proc 1988 summer program of center for turbulence research. NASA Ames/Stanford University; 1988. p. 193–207.
[35] Day M, Bell J, Cheng R, Tachibana S, Beckner V, Lijewski M. Cellular burning in lean premixed turbulent hydrogen-air flames: coupling experimental and computational analysis at the laboratory scale IOP Publishing J Phys Conf Ser 2009;180:012031.
[36] Turns SR. An introduction to combustion. New York: McGraw-hill; 1996.
[37] Aspden AJ. A numerical study of diffusive effects in turbulent lean premixed hydrogen flames. Proc Combust Inst 2017;36(2):1997–2004.